arXiv:0806.1548v1 [astro-ph] 9 Jun 2008

A Search for H_2CO 6 cm Emission toward Young Stellar Objects III: VLA Observations

E. D. Araya [1,2,3], P. Hofner[2,3], W. M. Goss[2], H. Linz[4], S. Kurtz[5] & L. Olmi[6,7]

ABSTRACT

We report the results of our third survey for formaldehyde (H_2CO) 6 cm maser emission in the Galaxy. Using the Very Large Array, we detected two new H_2CO maser sources (G23.01−0.41 and G25.83−0.18), thus increasing the sample of known H_2CO maser regions in the Galaxy to seven. We review the characteristics of the G23.01−0.41 and G25.83−0.18 star forming regions. The H_2CO masers in G23.01−0.41 and G25.83−0.18 share several properties with the other known H_2CO masers, in particular, emission from rich maser environments and close proximity to very young massive stellar objects.

Subject headings: ISM: molecules — masers — radio lines: ISM

[1]Department of Physics and Astronomy, MSC07 4220, University of New Mexico, Albuquerque, NM 87131

[2]National Radio Astronomy Observatory, P.O. Box 0, Socorro, NM 87801

[3]New Mexico Institute of Mining and Technology, Physics Department, 801 Leroy Place, Socorro, NM 87801

[4]Max–Planck–Institut für Astronomie, Königstuhl 17, D–69117 Heidelberg, Germany.

[5]Centro de Radioastronomía y Astrofísica, Universidad Nacional Autónoma de México, Apdo. Postal 3-72, 58089, Morelia, Michoacán, Mexico.

[6]University of Puerto Rico at Rio Piedras, Physics Department, P.O. Box 23343, San Juan, PR 00931.

[7]Istituto di Radioastronomia, INAF, Sezione di Firenze, Largo Enrico Fermi 5, I-50125 Florence, Italy.

1. Introduction

The first formaldehyde (H_2CO) 6 cm maser was discovered in 1974 toward NGC 7538 (Downes & Wilson 1974; Forster et al. 1980); in the following $\sim$ 28 years, H_2CO masers were detected only toward two other regions in the Galaxy: Sgr B2 (Whiteoak & Gardner 1983) and G29.96−0.02 (Pratap et al. 1994). This low number of H_2CO maser regions was unexpected (e.g., Forster et al. 1985; Gardner et al. 1986) given the detection of many H_2CO maser spots in a single source (Sgr B2, Whiteoak & Gardner 1983; Mehringer et al. 1994), the widespread distribution of formaldehyde molecules as exemplified by Galactic H_2CO 6 cm absorption (e.g., Watson et al. 2003; Araya et al. 2002; Downes et al. 1980; Dieter 1973), and the apparently common astrophysical conditions needed for the maser excitation if the masers were pumped by radio continuum radiation (see Pratap et al. 1992).

The idea that H_2CO masers may be pumped by background radio continuum was initially proposed by Boland & de Jong (1981) to explain the maser in NGC 7538 IRS1. However, the low detection rate of new H_2CO masers in dedicated surveys (Mehringer et al. 1995; Forster et al. 1985), the non-detection of maser emission from the H_2CO 2 cm transition (e.g., Hoffman et al. 2003) and low emission measure (or non-detection) of radio continuum sources near several of the known H_2CO masers, indicate that the pumping mechanism in most cases cannot be due to radio continuum excitation (e.g., see Araya et al. 2007c for the case of IRAS 18566+0408). The low detection rate of H_2CO masers led several authors to speculate that formaldehyde masers are rare because specific and/or short-lived physical conditions may be needed for the excitation (e.g., Forster et al. 1985; Mehringer et al. 1995; Araya et al. 2007a).

In an effort to understand the H_2CO maser phenomenon and its place during the formation of massive stars, we conducted two surveys for H_2CO masers using Arecibo, the Green Bank Telescope, and the VLA[1] that resulted in the detection of two new Galactic H_2CO maser regions (IRAS 18566+0408, with emission first detected by Araya et al. 2004 and confirmed to be a maser by Araya et al 2005; and G23.71-0.20 with details in Araya et al. 2006, from a survey later reported by Araya et al. 2007b). In this article we present the results of our third survey for H_2CO masers.

[1]The Very Large Array (VLA) is operated by the National Radio Astronomy Observatory (NRAO), a facility of the National Science Foundation operated under cooperative agreement by Associated Universities, Inc.

2. Observations

2.1. VLA Survey

The initial observations were conducted in 2006 June with the VLA during the BnA → B reconfiguration ($\theta_{syn} \sim 1.5''$). The details of the observations are reported in Table 1. A total of 14 pointing positions were observed toward massive star forming regions. In some cases, there were multiple radio continuum objects within the primary beam of a given position. Nine of the targets were selected based on their GBT and Arecibo spectra (Araya et al. 2002; Watson et al. 2003; Sewiło et al. 2004; Araya et al. 2007b) that showed profiles suggesting H_2CO emission blended with absorption. In addition, given that H_2CO 6 cm masers appear to originate mostly from regions that also harbor H_2O and Class II CH_3OH masers (e.g., Araya et al. 2005), we complemented our sample with 5 targets from the methanol and water maser catalog of Szymczak et al. (2005). The targets from the Szymczak et al. (2005) sample were observed ∼40 min on-source. In the case of the targets that were selected based on single dish H_2CO spectra, the time on-source ranged between 10 to 100 min depending on the expected intensity of the H_2CO emission line candidates. In Table 2 we list the observed targets, phase tracking center, center bandpass velocity, secondary (phase) calibrator used, and single-channel rms of the final data cubes. The data reduction and imaging were conducted using the NRAO package AIPS following the standard procedure for spectral line observations.

2.2. High Spectral Resolution Observations

Follow-up H_2CO 6 cm observations of G23.01−0.41 and G25.83−0.18 were conducted on 2007 February 16 with the VLA in the D configuration. The goals of the observations were to confirm the H_2CO 6 cm emission detected in our survey (§3), and to study the H_2CO maser line profiles with higher spectral resolution (1.83 kHz, 0.11 km s^{-1}). The VLA correlator was used in the 1 IF mode with a bandwidth of 0.78 MHz (48 km s^{-1}) and 512 channels. The central bandpass velocity was set to 70 and 87 km s^{-1} for the G23.01−0.41 and G25.83−0.18 observations, respectively. The phase tracking center of the G23.01−0.41 observations was RA = $18^{\rm h}34^{\rm m}40\overset{\rm s}{.}30$, Decl. = $-09^{o}00'00\overset{''}{.}0$ (J2000); the phase tracking center of the G25.83−0.18 observations was RA = $18^{\rm h}39^{\rm m}03\overset{\rm s}{.}60$, Decl. = $-06^{o}24'50\overset{''}{.}0$ (J2000). The quasars 3C286 and J1822−096 were used as primary and secondary calibrators, respectively. We assumed a flux density of 7.52 Jy for 3C286, and measured a flux density of 2.29 Jy for J1822−096. In addition, 3C48 was observed to check the flux density calibration. Using 3C286 as primary calibrator to bootstrap the flux density of 3C48, we measured a flux

density of 5.60 Jy for 3C48, which agrees within 3% with the expected value of 5.47 Jy. The calibration and imaging were conducted using the NRAO package AIPS.

3. Results

Of the 14 pointing positions observed with the VLA (and a total of 18 targets, see Table 2) we detected H_2CO 6 cm emission toward two sources: G23.01−0.41 and G25.83−0.18 (Figure 1). In both cases the emission was spatially unresolved (deconvolved size $< 0.5''$) implying brightness temperatures greater than 10^4 K, which indicates maser emission. Thus, G23.01−0.41 and G25.83−0.18 are the sixth and seventh regions in the Galaxy where H_2CO 6 cm masers have been detected.

Figure 1 shows the low velocity resolution spectra and peak channel images of the two new maser regions. The G23.01−0.41 line is spectrally unresolved whereas the H_2CO emission in G25.83−0.18 has a double peaked profile. Figure 2 shows the line profiles of the high spectral resolution (VLA-D, §2.2) observations. H_2CO emission was confirmed in both cases. In Table 3 we list the line parameters of the H_2CO 6 cm masers from both observing periods.

We detected radio continuum emission as well as H_2CO 6 cm absorption toward several of the targets in the sample; a discussion of these data will be the topic of a future paper. Here we focus on the H_2CO 6 cm maser emission, and discuss the H_2CO 6 cm absorption only in the case of G25.83−0.18 since the H_2CO maser originates at the (projected) spatial center of a molecular clump traced by H_2CO absorption (§4.2).

4. Discussion

4.1. G23.01−0.41

4.1.1. H_2CO 6 cm Maser Emission

H_2CO 6 cm maser emission was detected toward G23.01−0.41 with the VLA in the BnA → B reconfiguration (Figure 1), and confirmed with VLA-D observations conducted approximately 8 months later (§2.2, Figure 2). The peak position, LSR velocity, and line width measurements are consistent in both runs (Table 3). If the VLA-D spectrum is smoothed to the channel width of the lower spectral resolution observations (VLA BnA→B, Table 3), the peak intensities are consistent within 2σ, revealing no apparent variability of the line in

a ~ 8 month period.

As mentioned in §3, the H_2CO 6 cm maser in G23.01−0.41 was not spectrally resolved in the VLA BnA→B observations (line width < 1.0 km s^{-1}, Figure 1). In the high spectral resolution observations (Figure 2) the line was barely resolved, and appears to be the superposition of two components. The separation of the two possible overlapping lines is $\lesssim$0.4 km s^{-1}.

4.1.2. Infrared Environment

Far-IR emission is found at the location of the H_2CO maser as shown by IRAS data[2]. However, the far-IR emission at the H_2CO maser location is overlapped with several nearby sources. MSX 21.4μm data toward G23.01–0.41 is also affected by confusion due to blended emission with a source $\sim 20''$ east of the H_2CO maser position. At 70μm, MIPSGAL Spitzer data show that the maser is coincident with a compact (FWHM $< 30''$) and strong (saturated) FIR source. Since the emission is saturated, a reliable measurement of the 70 μm size and position cannot be obtained; nevertheless, the peak position appears to be within $\sim 3''$ of the H_2CO maser, i.e., certainly within the telescope angular resolution at 70 μm ($\sim 20''$; Rieke et al. 2004). At the 24 μm Spitzer MIPS band, the IR source coincident with the H_2CO maser is substantially less affected by saturation and the center position can be more reliably determined; the 24 μm source and the H_2CO maser are less that $0.3''$ apart.

The IR source coincident with the H_2CO maser is detected in mid/near-IR observations from the Spitzer/IRAC GLIMPSE survey (Benjamin et al. 2003). Figure 3 (upper panel) shows a three color image (3.6μm blue, 4.5μm green, 8.0μm red) of the G23.01−0.41 region. The Spitzer source at the H_2CO maser location shows strong 4.5μm excess indicative of shocked gas (e.g., Smith et al. 2006). There is also extended 4.5μm excess emission west of the H_2CO maser position (Figure 3, inset upper panel).

Testi et al. (1998) detected a near infrared (NIR) source toward G23.01−0.41, that was also detected by 2MASS. The 2MASS source is $\sim 4''$ displaced from the H_2CO maser position. Given this large angular offset, it is unlikely that the NIR source is responsible for the excitation of the masers in G23.01−0.41 (§4.1.4).

[2]IRSA-IRAS Sky Survey Atlas, http://irsa.ipac.caltech.edu/Missions/iras.html

4.1.3. Radio Continuum and Thermal Molecular Lines

We detected no 6 cm radio continuum toward the maser position to a 5σ level of 2.4 mJy beam^{-1} ($\theta_{syn} = 1\farcs6 \times 1\farcs1$). Using the VLA in the C configuration ($\theta_{sys} \sim 1''$), Codella et al. (1997) report an upper limit of the 1.3 cm radio continuum of 0.4 mJy beam^{-1} (3σ).

Based on our VLA-D observations, the nearest 6 cm radio continuum source is approximately 50″ north of the maser position. The radio continuum source (a compact H II region that will be discussed in a future paper) has associated H_2CO absorption at approximately the same velocity as the H_2CO maser, indicating that the H_2CO maser belongs to an extended molecular cloud that shows clear evidence for the presence of more evolved massive stars. The LSR velocity of the H_2CO absorption (75.0 km s^{-1}) implies two possible kinematic distances: 4.8 or 10.8 kpc. Codella et al. (1997) as well as Caswell & Haynes (1983) preferred the far kinematic distance[3]; however the distance ambiguity has not been resolved (Forster & Caswell 1999). For example, Harju et al. (1998) list the near kinematic distance for the source (see also Scoville et al. 1987, Pestalozzi et al. 2005).

A number of thermal molecular lines have been detected toward G23.01−0.41. Caswell et al. (2000) detected (quasi-)thermal emission of the CH_3OH lines at 107.0 GHz[4] and 156.6 GHz (see also Slysh et al. 1999). Harju et al. (1998) detected broad (line width > 20 km s^{-1}) SiO J=2–1 and J=3–2 emission with the SEST telescope. CO and ^{13}CO emission was also detected in single dish surveys (Scoville et al. 1987; Jackson et al. 2006).

Interferometric (Nobeyama Millimeter Array and Plateau de Bure Interferometer) observations of ^{12}CO, ^{13}CO, and $C^{18}O$ have been recently reported by Furuya et al. (2008) with an angular resolution ∼6″. Their ^{12}CO spectrum shows high velocity gas, in particular prominent red-wing emission that traces a massive ($> 50\,M_\odot$) molecular outflow, possibly located close to the plane of the sky.

High density molecular gas in the region is evident from detection of CS ($J = 1 - 0$) and NH_3 (1,1) lines with the MIT Haystack 37 m telescope (Anglada et al. 1996). Single dish NH_3 (1,1), (2,2), and (3,3) observations were also conducted by Codella et al. (1997) with the Medicina 32 m telescope. Codella et al. (1997) derived a rotational temperature of 13 K.

---

[3]Caswell & Haynes (1983; see also Caswell et al. 1995b, Anglada et al. 1996, Testi et al. 1998, Forster & Caswell 1999) report a far kinematic distance of 12.8 kpc instead of our value of 10.8 kpc because they assumed a Sun – Galactic Center distance of 10.0 kpc, whereas we assume 8.5 kpc (Brand & Blitz 1993).

[4]A maser component was also found superimposed on the thermal profile of the CH_3OH 107.0 GHz line.

High angular resolution NH_3 observations were conducted by Codella et al. (1997) with the VLA ($\theta_{syn} \sim 1''$). The NH_3 (3,3) data show a compact ($< 10''$) molecular core that has a SE–NW elongation (Figure 3, lower panel). Codella et al. (1997) derived the following parameters for the ammonia core: deconvolved angular diameter = $3\farcs3$, $T_k = 58\,K$, $M_{vir} = 886\,M_\odot$, and $n_{H_2} = 6.9 \times 10^6\,cm^{-3}$. The H_2CO maser is coincident with the NH_3 (3,3) peak emission (Figure 3, lower panel).

Furuya et al. (2008) recently conducted a detailed multi-wavelength study of G23.01−0.41 at high angular resolution ($< 10''$) using CO (see above), HNCO, and CH_3CN. Their observations confirm the presence of a hot molecular core characterized by a CH_3CN rotation temperature of $\sim 120\,K$ and a core mass of $\sim 380\,M_\odot$. The velocity distribution of the CH_3CN gas is consistent with rotation of a molecular core oriented almost perpendicular to the outflow direction. The elongation and velocity gradient of the CH_3CN core is parallel to the elongation of the NH_3 emission shown in Figure 3.

4.1.4. Other Astrophysical Masers

A variety of masers have been detected toward G23.01−0.41 in single dish surveys. Methanol masers have been found at 6.7 GHz (Menten 1991; Caswell et al. 1995b; Szymczak et al. 2002; see also catalogs by Pestalozzi et al. 2005 and Xu et al. 2003), 12 GHz (MacLeod et al. 1993; Caswell et al. 1995a; Błaszkiewicz & Kus 2004), 107.0 GHz (Caswell et al. 2000), 44 GHz (Slysh et al. 1994), and 95 GHz (Val'tts et al. 2000). H_2O 22 GHz and OH ($^2\Pi_{3/2}$ $J = 3/2$ ground state) masers have also been reported (Szymczak et al. 2005; Szymczak & Gérard 2004; Caswell & Haynes 1983).

High angular resolution observations of the CH_3OH 6.7 GHz masers have been conducted (Caswell, unpublished data; see Caswell et al. 2000); the position of the CH_3OH maser is coincident with that of the H_2CO maser within $1''$ rms. Forster & Caswell (1989, see also Forster & Caswell 1999) conducted VLA observations of H_2O 22 GHz ($\theta_{syn} = 3\farcs9 \times 1\farcs8$) and OH 1665 MHz ($\theta_{syn} = 6\farcs5 \times 1\farcs0$) masers in G23.01−0.41. The H_2CO maser is located within $2''$ of the OH and H_2O maser positions (see Figure 3 lower panel).

4.1.5. The Nature of the G23.01−0.41 Star Forming Region

The abundant available multi-wavelength data shows that G23.01−0.41 is an active site of massive star formation. The H_2CO maser is located at the peak of a molecular core traced by NH_3 (3,3) and CH_3CN. The hot molecular core also harbors a variety of

molecular masers. Given the highly confused far IR environment, it is not possible to reliably measure the bolometric luminosity of the massive stellar object pinpointed by the H_2CO maser (Figure 3); however, based on the available mid and far IR data, the upper limit of the luminosity is $\sim 10^6\,L_\odot$. As in the case of the infrared source associated with the H_2CO maser in IRAS 18566 + 0408 (Araya et al. 2007c), the H_2CO maser in G23.01−0.41 is found toward a source with 4.5μm infrared excess, which likely indicates shocked gas in an outflow. Considering the presence of a hot molecular core at the location of the H_2CO maser, the detection of several other maser species, evidence for outflow and shocked gas based on CO, SiO and 4.5μm infrared excess emission, absence of radio continuum, and evidence for rotation of the molecular core, the H_2CO maser appears to pinpoint the location of a very young massive stellar object in a evolutionary stage prior to the formation of a radio bright ultra-compact H II region. The central object may still be undergoing accretion; further observations should be made to clarify this point.

4.2. G25.83−0.18

4.2.1. H_2CO 6 cm Maser Emission

An the case of G23.01−0.41 (§4.1), maser emission in G25.83−0.18 was first detected in the VLA survey (§2.1) and then confirmed with higher spectral resolution observations (VLA-D, §2.2) $\sim$ 8 months later. The H_2CO maser shows a double peaked line profile (Figures 1 and 2). The separation between the two peak components is 1.5 km s^{-1}. No significant difference in the maser flux density was found between the two epochs.

As reported in Table 3, the line profile of the high spectral resolution observations is well fit by the superposition of three Gaussian profiles; two broad components (0.7 and 0.9 km s^{-1} FWHM) and a narrow component (FWHM = 0.29 km s^{-1}). Whether the line profile is composed of only two non-Gaussian maser lines or three (or more) components is unclear. For example, the profile could be due to an asymmetric line (the blue-shifted component) overlapped with a Gaussian line (the red-shifted component, see Figure 2).

4.2.2. Infrared Environment

The H_2CO maser is at the center of an infrared dark cloud as revealed by 8.0μm Spitzer/GLIMPSE observations (see Figure 4). The H_2CO maser is located between a source with strong 4.5μm excess emission (green in Figure 4, upper panel inset) and a source brighter at 8μm (red in Figure 4). The peak of the 4.5μm source is offset ($\sim 3''$) from the location of

the H_2CO maser. No infrared emission was detected with MSX toward the position of the H_2CO maser; no 2MASS source was found coincident with the H_2CO maser either.

Data from Spitzer MIPSGAL at 70μm reveal a strong (> 100 Jy) far IR source whose peak is within $\sim 1''$ from the position of the H_2CO maser. At low level, the 70μm emission is extended and comprises a neighboring infrared source; however, the core emission is compact (FWHM $< 25''$), i.e., close to the theoretical telescope diffraction limit. The IR source coincident with the H_2CO maser is also detected in the 24μm MIPS band.

4.2.3. Radio Continuum and Thermal Molecular Lines

We detected no radio continuum toward the position of the H_2CO maser to a level of 2.8 mJy beam^{-1} (5σ) in the VLA BnA $\rightarrow$ B observations ($\theta_{syn} = 1\farcs6 \times 1\farcs1$); the 5σ upper limit set by the VLA-D data is 5 mJy beam^{-1} (see Figure 4, upper panel). The nearest radio continuum source to the H_2CO maser is $\sim 2'$ to the west (G25.80$-$0.16; Figure 4, upper panel) which was also detected in the continuum at 8.64 and 6.67 GHz by Walsh et al. (1998).

The H_2CO maser is coincident with a mm and sub-mm core. Walsh et al. (2003) detected compact 450μm and 850μm emission; the H_2CO maser is located within $4''$ of the peak position of the sub-mm source (the JCMT beam is approximately $8''$ and $15''$ at 450μm and 850μm, respectively). Hill et al. (2005) conducted SEST/SIMBA observations of G25.83$-$0.18 and detected 1.2 mm emission ($S_\nu = 5.4$ Jy); the FWHM of the mm source is $60''$. Based on the mm detection, Hill et al. (2005) report a mass of 2.8×10^3 M$_\odot$ or 8.8×10^3 M$_\odot$ depending on the kinematic distance (see below). The H_2CO maser is coincident with the 1.2 mm peak within $\sim 1''$.

We detected H_2CO 6 cm absorption in the region (Figure 4, middle and lower panels, VLA-D observations). The main H_2CO absorption clump is coincident with the infrared dark cloud, and shows a shell-like brightness distribution (Figure 4, middle panel)[5]. The H_2CO maser is located at the projected spatial center of the shell and near the radial velocity edge of the H_2CO absorption line (Figure 4, lower panel). The shell brightness distribution could be due to: 1.) H_2CO in gas phase is less abundant in the inner regions of the shell, for example, due to chemical gradients, smaller total molecular density, or depletion (see Young et al. 2004 for the case of pre-protostellar cores); and/or 2.) the excitation conditions for H_2CO

[5]The shell-like distribution of H_2CO absorption (Figure 4, middle panel) is not due to overlapping H_2CO maser emission and absorption at the central position; the measured velocity of the H_2CO maser is not in the velocity range used to obtain the H_2CO absorption image.

absorption are less favorable in the inner regions of the clump (e.g., Zhou et al. 1990 explained the detection of an H_2CO shell-like structure in B335 as a consequence of higher molecular density at the core that quenches the anomalous absorption). Observations of other H_2CO transitions as well as other mid and high density tracers are needed to fully investigate the nature of the shell-like H_2CO absorption source. Nevertheless, the recent high angular resolution detection of NH_3 at the position of the H_2CO depression (Longmore et al. 2007, see below) suggests that the H_2CO shell-like structure is due to high density ($> 10^5\,cm^{-3}$) molecular gas in the center of the molecular core that quenches H_2CO anomalous absorption.

We also detected H_2CO absorption close to the radio continuum source (compare Figure 4 upper and middle panels). The similar velocity of the H_2CO absorption gas associated with the continuum source and with the infrared dark cloud indicates that both are part of the same star forming complex. Assuming that the LSR velocity of the H_2CO absorption line traces the systemic velocity of the cloud, the two possible kinematic distances to this massive star forming region are 5.6 and 9.7 kpc. Since the H_2CO maser is associated with an infrared cloud seen in absorption against the mid-IR galactic background (Figure 4), it is likely that the region is located at the near kinematic position.

G25.83−0.18 has been detected in CH_3CN, HCO^+, and $H^{13}CO^+$ with the Mopra telescope by Purcell et al. (2006). Based on the CH_3CN data, they derived a rotation temperature of ~ 50 K, and found evidence for infalling motion based on HCO^+ data. In addition, Longmore et al. (2007) detected an optically thick NH_3 core at the position of the H_2CO maser from ATCA observations. The line width of the NH_3 (1,1), (2,2), (4,4), and (5,5) transitions range between 6 and 30 km s^{-1}, indicating the possible presence of a molecular outflow partially traced by NH_3.

4.2.4. Other Astrophysical Masers

Walsh et al. (1998) conducted ATCA observations of 6.7 GHz CH_3OH masers in G25.83−0.18; five maser components were found with LSR velocities between of 90.7 and 99.0 km s^{-1}. The H_2CO maser is located $\sim 2''$ south of the CH_3OH maser clump[6] (Figure 4, upper panel, inset).

Single dish observations of the Class II CH_3OH 6.7 and 12 GHz masers were conducted by Błaszkiewicz & Kus (2004) with the Toruń telescope. The peak LSR velocity of the 6.7 and 12 GHz masers were 91.3 and 90.7 km s^{-1}, i.e., coincident in velocity with the H_2CO

[6]The absolute position accuracy of the CH_3OH masers is $\sim 1''$, Walsh et al. (1998).

maser.

Ellingsen (2005) conducted observations with the Mopra Telescope of the 95.1 GHz Class I CH_3OH maser transition, and detected several maser lines (peak maser emission at 90.2 km s^{-1}) overlapped with a broad component. The broad line (4.3 km s^{-1} line width) could be due to thermal emission given that its peak velocity (94.2 km s^{-1}) coincides with the H_2CO absorption peak velocity (see §4.2.3).

Other maser species have also been detected in single dish surveys. Szymczak & Gérard (2004) detected a OH 1667 MHz maser line with a peak LSR velocity of 92.9 km s^{-1}; their figure A.1 also shows detection of a possible high velocity ($\sim$ 120 km s^{-1}) OH 1612 MHz line. Szymczak et al. (2005) conducted H_2O 22 GHz observations with the 100 m Effelsberg telescope and detected several H_2O maser features within a velocity range of $\sim$ 50 km s^{-1}, centered at 94.7 km s^{-1}.

4.2.5. The Nature of the G25.83−0.18 Star Forming Region

The coincidence of the H_2CO maser with other maser species (in particular with Class II CH_3OH masers), with an infrared dark cloud and molecular core, the absence of radio continuum emission, the detection of a mm, sub-mm and far-IR source, and the presence of 4.5μm excess emission toward the center of the infrared dark cloud, imply that G25.83−0.18 is a very young region of massive star formation in an evolutionary stage prior to the ultra-compact H II region phase. The precise location and luminosity of the protostar responsible for the excitation of the different maser species is unclear; higher sensitivity continuum observations are needed to reveal the position of the exciting source. G25.83−0.18, as well as G23.01−0.41, may be classified as Group 2 cores following the Longmore et al. (2007) nomenclature, i.e., warm NH_3 cores associated with CH_3OH masers but no detectable radio continuum.

4.3. G23.01−0.41 and G25.83−0.18 with respect to the other known H_2CO Maser Regions

Including the two new masers reported in this work, H_2CO 6 cm masers have been detected toward seven regions in the Galaxy, and in a total of 15 maser 'spots' (at 1″ resolution). The H_2CO masers in G23.01−0.41 and G25.83−0.18 share similar characteristics with most of the other known H_2CO maser regions, in particular: (1.) H_2CO masers are found in regions that harbor a variety of other molecular masers (e.g., Hoffman et al. 2003;

Mehringer et al. 1994), (2.) the velocity difference of the H_2CO masers with respect to the systemic velocity of the clouds is typically less than 6 km s^{-1}(e.g., Pratap et al. 1994; Araya et al. 2004), which suggests that H_2CO masers do not originate in high velocity outflows, (3.) the flux density of the known masers is less than $\sim$2 Jy (e.g., Hoffman et al. 2007), (4.) all known H_2CO masers have been detected in regions of massive star formation (Araya et al. in prep.), (5.) excluding Sgr B2, most of the H_2CO masers show double peaked profiles with separations smaller than 3 km s^{-1} (e.g., NGC 7538 IRS1, Forster et al. 1985; IRAS 18566+0408, Araya et al. 2007d; see also review by Araya et al. 2007a), (6.) even though bright radio continuum sources may be found in the same star forming complexes, most H_2CO masers are located toward sources characterized by weak (or no) compact radio continuum emission, typically undetected at a few mJy sensitivity levels (e.g., Araya et al. 2005; this work), (7) excluding some of the masers in Sgr B2, the known H_2CO masers appear to be associated with very young massive stellar objects (in an evolutionary phase prior to the formation of radio-bright ultra-compact H II regions) that have strong far IR emission and molecular core counterparts (e.g., §4.1 and 4.2).

Many H_2CO maser regions show evidence of outflows/jets and shocked gas based on 4.5μm excess emission from Spitzer/IRAC data (see, for example, Araya et al. 2007c in the case of IRAS 18566+0408). Further evidence comes from molecular data such as SiO, H_2, and H_2S (e.g., Zhang et al. 2007; Beuther et al. 2007b; Kraus et al. 2006; Gibb et al. 2004; Maxia et al. 2001; Harju et al. 1998), and radio continuum observations (e.g., Araya et al. 2007c). However, the H_2CO masers may not be directly associated with the shocked material (e.g., note the offset between the 4.5μm excess source and the H_2CO maser in G25.83−0.18; Figure 4, upper panel).

5. Summary

We report the results of our third survey for H_2CO 6 cm masers toward massive star forming regions in the Galaxy. The observations were conducted with the VLA toward 14 pointing positions, and resulted in the detection of two new H_2CO maser regions: G23.01−0.41 and G25.83−0.18. Including the new detections, H_2CO masers have been found toward a total of seven star forming regions in the Galaxy, four of them detected in our series of surveys (Araya et al. 2004, 2007b, and this work).

The H_2CO maser in G23.01−0.41 is coincident with the center of a hot molecular core that shows evidence of a rotating torus perpendicular to a molecular outflow (Furuya et al. 2008). Excess in the 4.5 μm band from GLIMPSE Spitzer/IRAC observations reveals shocked gas in the region, possibly tracing the outflow. Active massive star formation is also evident from the detection of a number of molecular maser lines, including Class II CH_3OH

masers.

In the case of G25.83−0.18, the maser is located at the center of an infrared dark cloud that harbors a clump of CH_3OH 6.7 GHz masers, a high density molecular core traced by NH_3 and CH_3CN (Purcell et al. 2006), a mm, sub-mm and far IR counterpart. In addition there is evidence for molecular infall and outflow motions, as well as shocked gas traced by 4.5 μm excess from Spitzer GLIMPSE data.

In both cases the H_2CO masers are found toward objects that have no compact 6 cm radio continuum emission at the few mJy/beam level. Given the evidence of active massive star formation in G23.01−0.41 and G25.83−0.18, the absence of radio continuum suggests that the regions are in a very early phase of massive star formation, prior to the development of radio-bright ultra-compact H II regions. H_2CO 6 cm masers appear to preferentially pinpoint very young massive stellar objects that may be categorized as HMPOs (High-Mass Protostellar objects, Beuther et al. 2007a) or, in the Zinnecker & Yorke (2007) nomenclature, somewhere in the HDMC (Hot Dense Massive Core) or DAMS (disk-accreting main-sequence star) phase.

E. A. is supported by a NRAO predoctoral fellowship. H. L. was supported by a postdoctoral stipend from the German Max Planck Society. L. O. was supported in part by the Puerto Rico Space Grant Consortium. We thank the anonymous referee for comments that improved the manuscript. This research made use of the NASA's Astrophysics Data System, the Avedisova (2002) catalog, the VizieR catalog access tool (CDS, Strasbourg, France), and archival data from the *Spitzer Space Telescope*. The *Two Micron All Sky Survey* catalog was also consulted as part of this investigation; 2MASS is a joint project of the University of Massachusetts and the Infrared Processing and Analysis Center/California Institute of Technology, funded by NASA and the National Science Foundation.

REFERENCES

Anglada, G., Estalella, R., Pastor, J., Rodríguez, L. F., & Haschick, A. D. 1996, ApJ, 463, 205

Araya, E., Hofner, P., Churchwell, E., & Kurtz, S. 2002, ApJS, 138, 63

Araya, E., Hofner, P., & Goss, W. M. 2007a, in Astrophysical Masers and their Environments, IAU Symp. 242, ed. J. Chapman, & W. A. Baan, (Cambridge: Cambridge Univ. Press), 110 (arXiv:0707.1841)

Araya, E., Hofner, P., Goss, W. M., Kurtz, S., Linz, H., & Olmi, L. 2006, ApJ, 643, L33

Araya, E., Hofner, P., Goss, W. M., Linz, H., Kurtz, S., & Olmi, L. 2007b, ApJS, 170, 152

Araya, E., Hofner, P., Kurtz, S., Linz, H., Olmi, L., Sewiło, M., Watson, C., & Churchwell, E. 2005, ApJ, 618, 339

Araya, E., Hofner, P., Linz, H., Sewiło, M., Watson, C., Churchwell, E., Olmi, L., & Kurtz, S. 2004, ApJS, 154, 579

Araya, E., et al. 2007c, ApJ, 669, 1050

Araya, E., Hofner, P., Sewiło, M., Linz, H., Kurtz, S., Olmi, L., Watson, C. & Churchwell, E. 2007d, ApJ, 654, L95

Avedisova, V. S. 2002, Astro. Rep. 46, 193

Benjamin, R. A., et al. 2003, PASP, 115, 953

Beuther, H., Churchwell, E. B., McKee, C. F., & Tan, J. C. 2007a, in Protostars & Planets V, ed. B. Reipurth, D. Jewitt, & K. Keil (Tucson: Univ. of Arizona Press), 165

Beuther, H., Zhang, Q., Bergin, E. A., Sridharan, T. K., Hunter, T. R., & Leurini, S. 2007b, A&A, 468, 1045

Błaszkiewicz, L., & Kus, A. J. 2004, A&A, 413, 233

Boland, W., & de Jong, T. 1981, A&A, 98, 149

Brand, J., & Blitz, L. 1993, A&A, 275, 67

Caswell, J. L., & Haynes, R. F. 1983, Aust. J. Phys., 36, 417

Caswell, J. L., Yi, J., Booth, R. S., & Cragg, D. M. 2000, MNRAS, 313, 599

Caswell, J. L., Vaile, R. A., Ellingsen, S. P., & Norris, R. P. 1995a, MNRAS, 274, 1126

Caswell, J. L., Vaile, R. A., Ellingsen, S. P., Whiteoak, J. B., & Norris, R. P. 1995b, MNRAS, 272, 96

Codella, C., Testi, L., & Cesaroni, R. 1997, A&A, 325, 282

Dieter, N. H. 1973, ApJ, 183, 449

Downes, D., & Wilson, T. L. 1974, ApJ, 191, L77

Downes, D., Wilson, T. L., Bieging, J., & Wink, J. 1980, A&AS, 40, 379

Ellingsen, S. P. 2005, MNRAS, 359, 1498

Forster, J. R., & Caswell, J. L. 1999, A&AS, 137, 43

Forster, J. R., & Caswell, J. L. 1989, A&A, 213, 339

Forster, J. R., Goss, W. M., Gardner, F. F., & Stewart, R. T. 1985, MNRAS, 216, 35

Forster, J. R., Goss, W. M., Wilson, T. L., Downes, D., & Dickel, H. R. 1980, A&A, 84, L1

Furuya, R. S., Cesaroni, R., Takahashi, S., Codella, C., Momose, M., Beltrán, M. T. 2008, ApJ, 673, 363 (arXiv: 0710.0029)

Gardner, F. F., Whiteoak, J. B., Forster, J. R., & Pankonin, V. 1986, MNRAS, 218, 385

Gibb, A. G., Wyrowski, F., & Mundy, L. G., 2004, ApJ, 616, 301

Harju, J., Lehtinen, K., Booth, R. S., & Zinchenko, I. 1998, A&AS, 132, 211

Hill, T., Burton, M. G., Minier, V., Thompson, M. A., Walsh, A. J., Hunt-Cunningham, M., & Garay, G. 2005, MNRAS, 363, 405

Hoffman, I. M., Goss, W. M., & Palmer, P. 2007, ApJ, 654, 971

Hoffman, I. M., Goss, W. M., Palmer, P., & Richards, A. M. S. 2003, ApJ, 598, 1061

Jackson, J. M., et al. 2006, ApJS, 163, 145

Kraus, S., Balega, Y., Elitzur, M., Hofmann, K.-H., Preibisch, Th., Rosen, A., Schertl, D., Weigelt, G., & Young, E. T. 2006, A&A, 455, 521

Longmore, S. N., Burton, M. G., Barnes, P. J., Wong, T., & Purcell, C. R. 2007, MNRAS, 379, 535

MacLeod, G. C., Gaylard, M. J., & Kemball, A. J. 1993, MNRAS, 262, 343

Maxia, C., Testi, L., Cesaroni, R., & Walmsley, C. M. 2001, A&A, 371, 287

Mehringer, D. M., Goss, W. M., & Palmer, P. 1994, ApJ, 434, 237

Mehringer, D. M., Goss, W. M., & Palmer, P. 1995, ApJ, 452, 304

Menten, K. M. 1991, ApJ, 380, L75

Pestalozzi, M. R., Minier, V., & Booth, R. S. 2005, A&A, 432, 737

Pratap, P., Menten, K. M., & Snyder, L. E. 1994, ApJ, 430, L129

Pratap, P., Snyder, L. E., & Batrla, W. 1992, ApJ, 387, 241

Purcell, C. R., et al. 2006, MNRAS, 367, 553

Rieke et al. 2004, ApJS, 154, 25

Scoville, N. Z., Su Yun, M., Clemens, D. P., Sanders, D. B., & Waller, W. H. 1987, ApJS, 63, 821

Sewiło, M., Watson, C., Araya, E., Churchwell, E., Hofner, P., & Kurtz, S. 2004, ApJS, 154, 553

Slysh, V. I., Kalenskii, S. V., Val'tts, I. E., Golubev, V. V., & Mead, K. 1999, ApJS, 123, 515

Slysh, V. I., Kalenskii, S. V., Val'tts, I. E., & Otrupcek, R. 1994, MNRAS, 1994, 268, 464

Smith, H. A., Hora, J. L., Marengo, M., & Pipher, J. L. 2006, ApJ, 645, 1264

Szymczak, M., & Gérard, E. 2004, A&A, 414, 235

Szymczak, M., Kus, A. J., Hrynek, G., Kępa, A. & Pezderski, E. 2002, A&A, 392, 277

Szymczak, M., Pillai, T., & Menten, K. M. 2005, A&A, 434, 613

Testi, L., Felli, M., Persi, P., & Roth, M. 1998, A&AS, 129, 495

Tucker, K. D., Tomasevich, G. R., & Thaddeus, P. 1970, ApJ, 161, L153

Val'tts, I. E., Ellingsen, S. P., Slysh, V. I., Kalenskii, S. V., Otrupcek, R., & Larionov, G. M. 2000, MNRAS, 317, 315

Walsh, A. J., Burton, M. G., Hyland, A. R., & Robinson, G. 1998, MNRAS, 301, 640

Walsh, A. J., Macdonald, G. H., Alvey, N. D. S., Burton, M. G., & Lee, J.-K. 2003, A&A, 410, 597

Watson, C., Araya, E., Sewiło, M., Churchwell, E., Hofner, P., & Kurtz, S. 2003, ApJ, 587, 714

Whiteoak, J. B., & Gardner, F. F. 1983, MNRAS, 205, 27

Xu, Y., Zheng, X.-W., & Jiang, D.-R. 2003, Chin. J. Astron. Astrophys., 3, 49

Young, K. E., Lee, J.-E., Evans II, N. J., Goldsmith, P. F., & Doty, S. D. 2004, ApJ, 614, 252

Zhang, Q., Sridharan, T. K., Hunter, T. R., Chen, Y., Beuther, H., & Wyrowski, F. 2007, A&A, 470, 269

Zhou, S., Evans II, N. J., Butner, H. M., Kutner, M. L., Leung, C. M., & Mundy, L. G. 1990, ApJ, 363, 168

Zinnecker, H., & Yorke, H. W. 2007, ARA&A, 45, 481

This preprint was prepared with the AAS LaTeX macros v5.2.

Table 1. VLA H_2CO Survey

Parameter	Value
Date	2006 Jun. 13 - 15
Configuration[a]	BnA→B
ν_o (GHz)[b]	4829.6594
IF Mode	2IF (AD)
BW (MHz)[c]	1.56
(km s^{-1})	97.0
$\Delta\nu^d$ (kHz)	7.3
(km s^{-1})	0.46
Flux Density Calib.	3C 286
Assumed S_ν (Jy)	7.52
Phase Calib.	J1832−105
Measured S_ν (Jy)	1.26
Phase Calib.	J1824+107
Measured S_ν (Jy)	0.80
Phase Calib.	J1950+081
Measured S_ν (Jy)	1.07

[a]Reconfiguration from BnA to B array.

[b]Weighted average frequency of the H_2CO $J_{K_aK_c} = 1_{10} - 1_{11}$ $F = 2 - 2$ and $F = 0 - 1$ hyperfine transitions given in Tucker et al. (1970).

[c]Bandwidth per IF.

[d]Spectral resolution.

Table 2. Observed Targets.

Target	$\alpha(2000)^{\blacklozenge}$ (h m s)	$\delta(2000)^{\blacklozenge}$ (^{o} $'$ $''$)	$V^{\diamond}_{LSR}$ (km s^{-1})	Phase Calib.	rms‡ (mJy)
G13.13−0.15	18 14 41.27	−17 37 04.2	40.0	J1832−105	7.6
G13.21−0.14	†	†	40.0	J1832−105	17.4
G21.57−0.03	18 30 36.50	−10 06 44.0	110.0	J1832−105	5.7
G22.05+0.22	18 30 35.70	−09 34 26.0	50.0	J1832−105	5.2
G22.36+0.06	18 31 44.84	−09 22 08.5	85.0	J1832−105	4.9
G23.01−0.41	18 34 40.60	−09 00 28.0	75.0	J1832−105	6.2
G22.97−0.39	⋆	⋆	75.0	J1832−105	5.4
G24.68−0.16	18 36 51.80	−07 24 48.3	50.0	J1832−105	4.6
G25.79−0.14	18 38 51.73	−06 25 00.6	100.0	J1832−105	4.9
G25.80−0.16	∗	∗	100.0	J1832−105	5.2
G25.83−0.18	∗	∗	100.0	J1832−105	6.7
G27.28+0.15	18 40 33.90	−04 57 18.0	35.0	J1832−105	5.6
G30.87+0.11	18 47 15.76	−01 47 10.3	90.0	J1832−105	10.1
G33.92+0.11	18 52 50.27	+00 55 29.6	100.0	J1824+107	4.8
G37.87−0.40	19 01 53.57	+04 12 49.2	60.0	J1824+107	5.6
G39.10+0.48	19 00 59.50	+05 42 28.0	15.0	J1824+107	5.9
G42.43−0.26	19 09 50.08	+08 19 39.7	60.0	J1950+081	3.6
G43.26−0.21	19 11 05.74	+09 05 06.0	60.0	J1950+081	9.3

Note. — $^{(\blacklozenge)}$ Phase tracking center. $^{(\diamond)}$ Center bandpass LSR velocity. $^{(\ddagger)}$ Single channel rms of the final H_2CO data cube. $^{(\dagger)}$ G13.21−0.14 was included in the VLA primary beam of G13.13−0.15. The reported rms was obtained toward the G13.21−0.14 position after correcting for primary beam attenuation. $^{(\star)}$ G22.97−0.39 was included in the VLA primary beam of G23.01−0.41. The reported rms was obtained toward the G22.97−0.39 position after correcting for primary beam attenuation. $^{(*)}$ G25.83−0.18 and G25.80−0.16 were included in the VLA primary beam of G25.79−0.14. The reported rms values were obtained toward the G25.83−0.18 and G25.80−0.16 positions after correcting for primary beam attenuation.

Table 3. Line Parameters of H_2CO 6 cm Masers

Source	α_{peak}(J2000) (h m s)	δ_{peak}(J2000) (^{o} $'$ $''$)	$I_{\nu,peak}$ (mJy/b)	V_{LSR} (km s^{-1})	FWHM (km s^{-1})
VLA BnA → B (Low Spectral Resolution) Observations					
G23.01−0.41†	18 34 40.294(0.004)	−09 00 38.26(0.08)	48(6)	73.5(0.4)	<1.0
G25.83−0.18‡	18 39 03.627(0.003)	−06 24 11.18(0.06)	85(7)	90.2(0.4)	<0.8
			45(7)	91.4(0.1)	1.8(0.3)
VLA-D (High Spectral Resolution) Observations					
G23.01−0.41*	18 34 40.29(0.06)	−09 00 37.7(1.3)	53(9)	73.60(0.09)	0.4(0.2)
G25.83−0.18*	18 39 03.69(0.07)	−06 24 10.4(0.8)	102(9)	90.21(0.02)	0.29(0.04)
			52(9)	91.64(0.08)	0.9(0.2)
			44(9)	90.6(0.1)	0.7(0.3)

Note. — Unless indicated otherwise, we list the intensity of the peak channel (the rms is listed as uncertainty), the LSR velocity of the peak channel (channel separation reported as uncertainty), and the FWHM (two times the channel separation is reported as uncertainty). $^{(\dagger)}$ $\theta_{syn} = 1\farcs6 \times 1\farcs1$, P.A. $= -7^o$. ‡ $\theta_{syn} = 1\farcs6 \times 1\farcs1$, P.A. $= -18^o$. The line parameters of the weak component were derived from a Gaussian fit. $^{(*)}$ $\theta_{syn} = 21'' \times 12''$, P.A. $= -13^o$. $^{(\star)}$ $\theta_{syn} = 23'' \times 15''$, P.A. $= -8^o$. The line parameters were obtained from a three component Gaussian fit; the intensity and velocity of the two peak channels are: (113 mJy beam^{-1}, 90.2 km s^{-1}) and (66 mJy beam^{-1}, 91.7 km s^{-1}); see Figure 2.

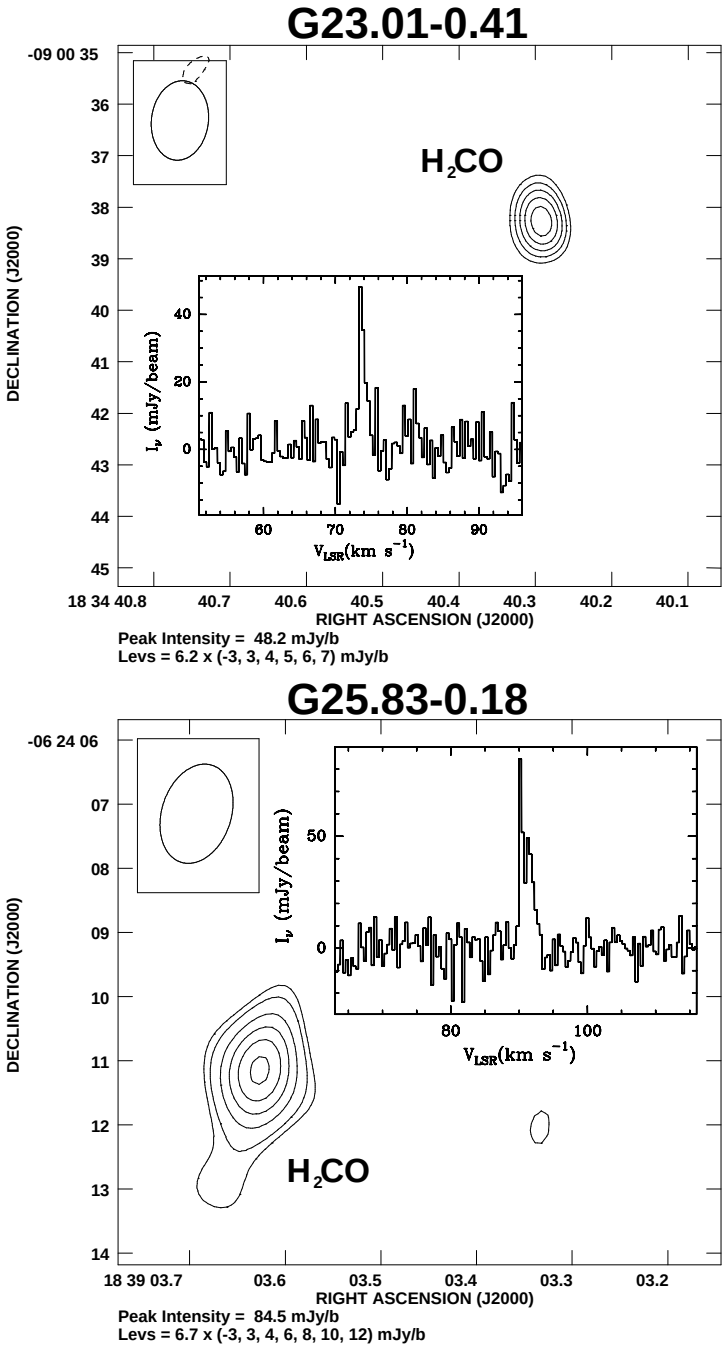

Fig. 1.— Detection of H_2CO 6 cm masers toward G23.01−0.41 (rms = 6.2 mJy beam^{-1}; $\theta_{syn} = 1\farcs6 \times 1\farcs1$, P.A. = -7^o) and G25.83−0.18 (rms = 6.7 mJy beam^{-1}; $\theta_{syn} = 1\farcs6 \times 1\farcs1$, P.A. = -18^o). The peak channel images are shown in contours and the spectra are shown in the insets. The observations were conducted in 2006 June (see §2.1), with a spectral resolution of 0.46 km s^{-1}.

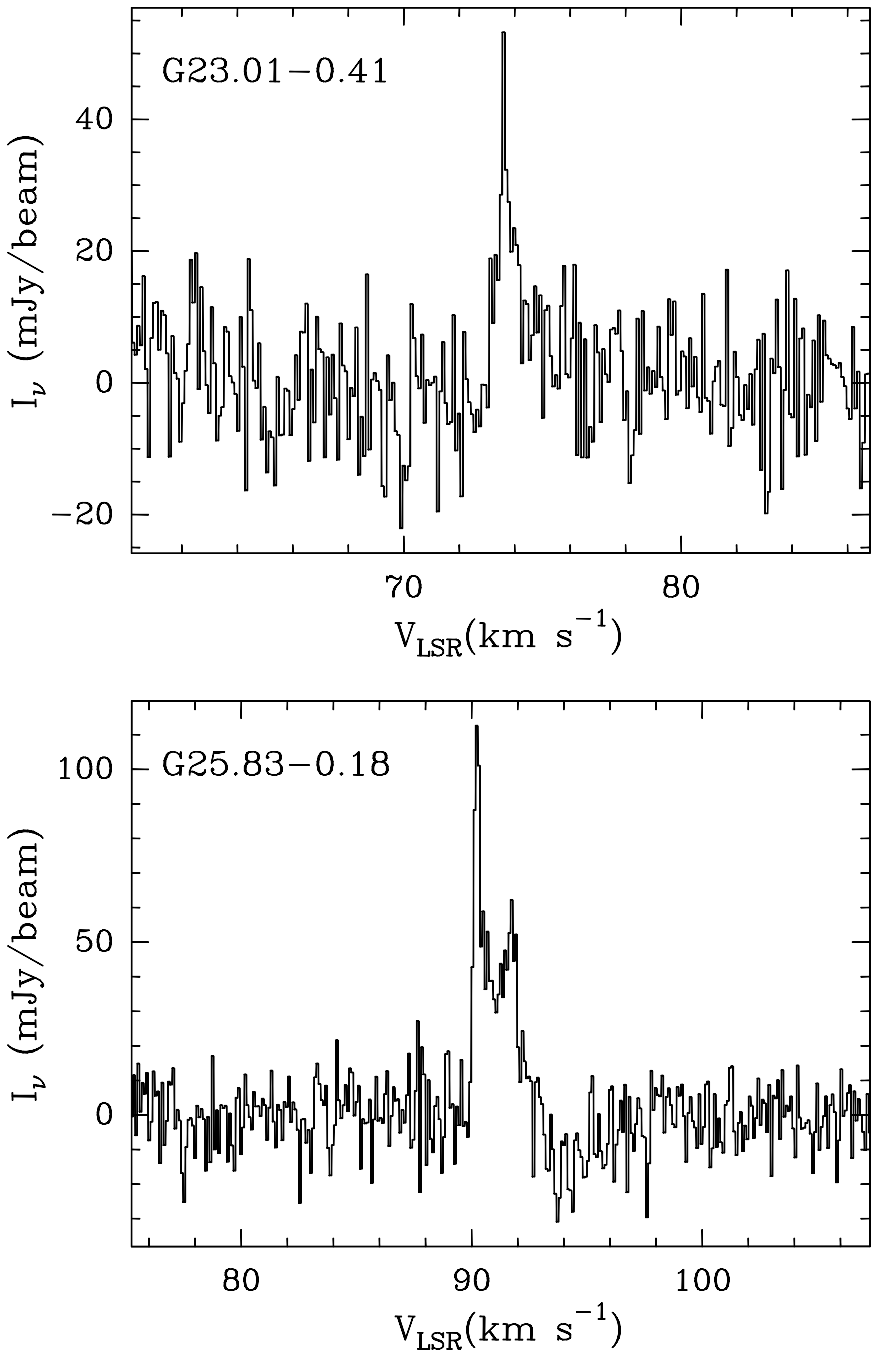

Fig. 2.— High spectral resolution (0.11 km s^{-1}) VLA-D observations of the H_2CO 6 cm masers in G23.01−0.41 and G25.83−0.18. The G25.83−0.18 H_2CO spectrum has a clear double peaked profile; the line profile of the maser in G23.01−0.41 also appears to be the superposition of 2 lines. The observations were conducted in 2007 February (§2.2).

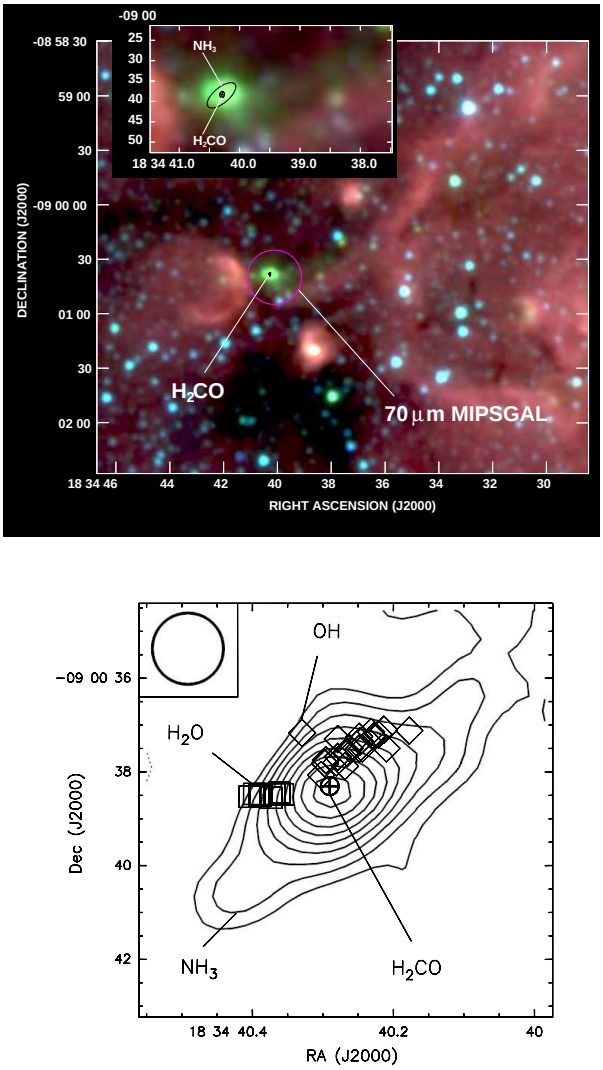

Fig. 3.— *Upper Panel:* Spitzer/IRAC GLIMPSE three-color image of the G23.01−0.41 region; the 3.6, 4.5, and 8.0μm bands are shown in blue, green, and red, respectively. The location and FWHM upper limit of the 70 μm MIPSGAL counterpart is shown with a magenta circle (see §4.1.2). A closeup of the G23.01−0.41 region is shown in the inset. Note the strong 4.5 μm excess toward the H_2CO maser that extends westwards. The ellipse represents the approximate size and position angle of the NH_3 core shown in the lower panel (size, position and orientation of the ellipse are from a fit of the 12 mJy beam^{-1} contour of the Codella et al. (1997) map). The location of the H_2CO maser is explicitly marked in all panels. *Lower Panel:* Zoomed-in view of G23.01−0.41. The contours show the NH_3 (3,3) emission imaged with the VLA by Codella et al. (1997; the original VLA image was convolved with a Gaussian profile whose FWHM is shown in the upper-left corner of the figure). The location of H_2O (22 GHz) and OH (1665 MHz) masers from Forster & Caswell (1999) are marked with squares and diamonds, respectively. The absolute astrometry of the OH and H_2O maser positions is $\sim 0\farcs5$ rms (see Forster & Caswell 1999).

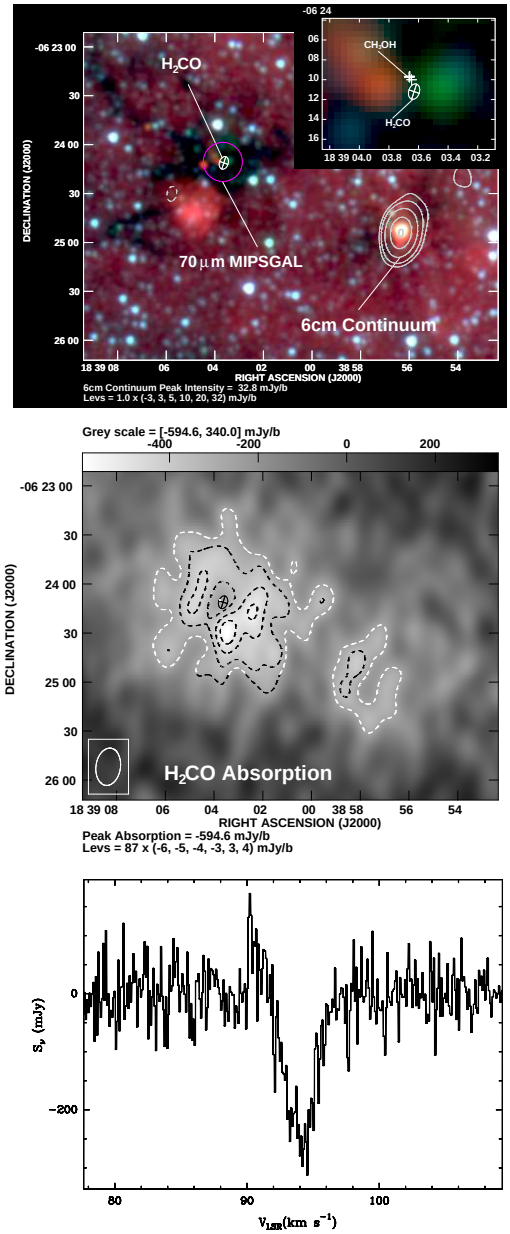

Fig. 4.— *Upper panel:* We show in contours the radio continuum (6 cm) image of the G25.83−0.18 region (rms = 1 mJy beam^{-1}; θ_{syn} = 23.″0 × 15.″0, P.A. = -8^o) superimposed on a Spitzer/IRAC GLIMPSE three-color image of the region (3.6μm blue, 4.5μm green, and 8.0μm red). The location and FWHM upper limit of the 70 μm counterpart is shown with a magenta circle (see §4.2.2). A zoomed-in view of the H_2CO maser region is shown in the inset; the position of CH_3OH 6.7 GHz masers are also shown (Walsh et al. 1998; absolute position accuracy $\sim$ 1″). *Middle Panel:* Sum of the channel maps in the 92.4 to 95.5 km s^{-1} velocity range. The position of the H_2CO maser is shown with a '$\oplus$' symbol in the upper and middle panels; the orientation of the symbol represents the P.A. of the θ_{syn} and its size is five times the size of the θ_{syn} (§2.1, Table 3). In the inset of the upper panel, the size of the symbol is that of the VLA synthesized beam. *Lower Panel:* Spectrum of the G25.83−0.18 maser region obtained by integrating the brightness distribution in a 85″×90″ area centered at the H_2CO maser position. Note the maser emission at $\sim$ 90 km s^{-1}.